Accurate Endocardial Activation Representation of Atria by Noncontact Mapping

Shu Meng[1], Jichao Zhao[1], Brett M Burton[2], Nigel A Lever [1,3,5], Ian J LeGrice[1,4], Bruce H Smaill[1, 4]

[1]Auckland Bioengineering Institute, University of Auckland, Auckland, New Zealand
[2]Department of Bioengineering, University of Utah, Salt Lake City, USA
[3]Medicine and [4]Physiology, University of Auckland, Auckland, New Zealand
[5]Auckland City Hospital, Auckland, New Zealand

Abstract

Atrial fibrillation (AF) is the most common heart rhythm disturbance. Percutaneous catheter ablation has been less defined for patients with persistent AF (PeAF) even with optimally combined ablation approaches. The fundamental reason behind that is lack of knowledge on functional and anatomic substrates of PeAF and effective electrical mapping tools. To address this, our group aims to develop a novel high resolution noncontact multi-electrode array (MEA) mapping system that could map electrical activation in two atrial chambers simultaneously. Here, in this study, we explore the relationship between the electrical potentials recorded by MEA and actual ones at atrial endocardial surfaces by solving forward and inverse problems in a nutshell. Our results demonstrate that the potential-based forward/inverse method provides robust electrical transformation between MEAs and smoothed atrial anatomical structure.

1. Introduction

Treatment of atrial fibrillation (AF) is an increasing economic burden in health care [1]. Percutaneous catheter ablation is widely used to treat patients with AF and has achieved great success [2]. The most common AF ablation techniques are pulmonary vein isolation, which have achieved more than 80% success rate for paroxysmal AF, and ablation guided by identifying specific substrates that may give rise to reentrant arrhythmia, less defined approach for treatment of persistent AF (PeAF) (long term success rate is only ~28.4% after a single ablation procedure) [3,4]. Reasons for latter are that functional and anatomic substrates play an important role in sustaining PeAF [5], and current techniques for substrate identification in PeAF are relatively ineffective [6].

Identification of AF substrates with current mapping technologies presents a number of problems. With contact mapping systems [6] (Biosense Webster Inc.), it is necessary to acquire sequential electrograms region-by-region across the endocardial surfaces of the atrial chambers. However, it is difficult to reconstruct repeatable activation patterns in AF, because electrical activity is nonstationary. An alternative approach is to reconstruct extracellular electrograms on the endocardial surface of the atria from electrical recordings acquired from noncontact multi-electrode arrays (MEAs) [6,7]. This provides a simultaneous view of global electric activity, which is crucial for accurate dynamic analysis of AF. Currently, there are renewed interests in this area academically and commercially [7,8]. A recent clinical pilot trial (CONFIRM) [8] using a noncontact MEA suggests that significantly higher success of catheter ablation could be achieved with systematic identification of focal sources and rotors.

However, how to relate atrial electrograms recorded at basket electrodes to specific anatomical sites of atrial endocardial surface accurately is a challenging problem. One way is to use impedance techniques, which do not relate well to high accurate anatomy obtained with established 3D imaging modalities, e.g., CT or MRI [9]. In this work, we have investigated relationship between potentials recorded by MEAs and actual ones at atrial endocardial surface by solving a forward/inverse problem in a nutshell using finite difference method (FDM). Our focus here is to test the main concepts. Throughout the paper, we only discuss "potential-based" source model.

2. Methods

In this section, firstly, we will illustrate the principle of forward and inverse problems by deriving forward/inverse equations using FDM. Secondly, the procedure and methods we used to reconstruct 3D endocardial surface of the atria are explained. Lastly, forward problems are tested on the realistic 3D left atrial

(LA) endocardial surface and MEAs.

2.1. The forward and inverse problems

Forward and inverse problems of electrocardiography have been studies extensively [10]. The forward problem is to project electrical potentials from source, through some medium, to another object. The solution to inverse problem is to predict electrical sources given a set of measurements obtained on the other geometry.

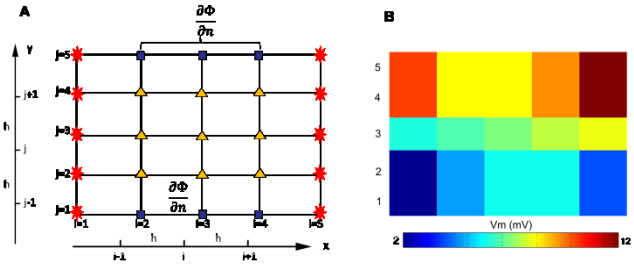

Figure 1: (A) Grid partition schematic for the 2D domain used for illustration of the forward and inverse problems (h = 1/4). Source is located at i=1 and i=5, and Neumann condition is superimposed at j=1 and j=5. (B) The forward solutions are displayed at the 5×5 grid nodes. Here the colour spectrum is used to indicate potentials.

The potential-based model is governed by the Laplace Equation at $\Omega = [0,1] \times [0,1]$ (Figure 1):

$$\sigma_x \frac{\partial^2 \Phi}{\partial x^2} + \sigma_y \frac{\partial^2 \Phi}{\partial y^2} = 0, \ [x, y] \in \Omega \quad (1)$$

Here $\sigma = [\sigma_x, \sigma_y]$ denotes the relevant conductivity, and $\Phi(x, y)$ is the electrical potentials. The Dirichlet boundary conditions around source ($x = 0$ and $x = 1$) are given explicitly by:

$$\Phi(x, y)|_{\Omega_s} = D_s \quad (2)$$

Neumann condition at Ω_N ($y = 0$ and $y = 1$) is:

$$\frac{\partial \Phi}{\partial n}|_{\Omega} = 0 \quad (3)$$

The most common used approaches for forward/inverse problems nowadays are FDM, finite element method (FEM) and boundary element method (BEM). FDM offers a simple and straightforward way to deal with the numerical problems [11]. In this section, we try to avoid complex mathematical equations and matrices, instead we adopt a simple 2D test problem to illustrate how to solve forward and inverse problems numerically. To solve equation (1), any interior grid node $\Phi_{i,j}$ needs keeping itself updated recursively using the following equation derived by central difference scheme ($\sigma = 1$ for simplicity):

$$\Phi_{i,j} = \frac{1}{4}[\Phi_{i+1,j} + \Phi_{i-1,j} + \Phi_{i,j+1} + \Phi_{i,j-1}], \ i/j=2,3,4 \quad (4)$$

Discretizing Neumann condition yields:

$$\Phi_{i,1} = \Phi_{i,2}, \quad \Phi_{i,5} = \Phi_{i,4}, \quad i = 2,3,4 \quad (5)$$

Using the numerical scheme (4) and boundary conditions (2,5), we could obtain the following matrix equation:

$$\begin{pmatrix} A_3 & I_3 & 0 \\ I_3 & A_4 & I_3 \\ 0 & I_3 & A_3 \end{pmatrix}_{9\times 9} \begin{pmatrix} \Phi_{2,2} \\ \vdots \\ \Phi_{44} \end{pmatrix}_9 = \begin{pmatrix} I' & 0 & 0 \\ 0 & I' & 0 \\ 0 & 0 & I' \end{pmatrix}_{9\times 6} \begin{pmatrix} \Phi_{1,2} \\ \vdots \\ \Phi_{5,4} \end{pmatrix}_6 \quad (6)$$

The left side contains interior grid nodes, while the right side has only grid nodes at Dirichlet boundary conditions (the source). Here I_3 is a 3×3 identity matrix, and

$$A_k = \begin{pmatrix} k & 1 & 0 \\ 1 & k & 1 \\ 0 & 1 & k \end{pmatrix}_{3\times 3} \quad \text{k=3 or 4;} \quad I' = \begin{pmatrix} 1 & 0 \\ 0 & 0 \\ 1 & 1 \end{pmatrix}_{3\times 2} \quad (7)$$

Note that A_k are positive definite matrices. The relation between grid nodes at Neumann boundary conditions (the measured potentials) and interior grid nodes could be been rewritten into matrix form:

$$\begin{pmatrix} \Phi_{2,1} \\ \vdots \\ \Phi_{4,5} \end{pmatrix}_6 = \begin{pmatrix} I_3 & 0 & 0 \\ 0 & 0 & I_3 \end{pmatrix}_{6\times 9} \begin{pmatrix} \Phi_{2,2} \\ \vdots \\ \Phi_{4,4} \end{pmatrix}_9 \quad (8)$$

Thus by combining (6-8) equations, we could have the following forward equation:

$$Y = AX \quad (9)$$

Here,

$$Y = \begin{pmatrix} \Phi_{2,1} \\ \vdots \\ \Phi_{4,5} \end{pmatrix}_6, \quad X = \begin{pmatrix} \Phi_{1,2} \\ \vdots \\ \Phi_{5,4} \end{pmatrix}_6,$$

$$A = \begin{pmatrix} I_3 & 0 & 0 \\ 0 & 0 & I_3 \end{pmatrix} \begin{pmatrix} A_3 & I_3 & 0 \\ I_3 & A_4 & I_3 \\ 0 & I_3 & A_4 \end{pmatrix}^{-1} \begin{pmatrix} I' & 0 & 0 \\ 0 & I' & 0 \\ 0 & 0 & I' \end{pmatrix}$$

Once the forward matrix A is determined, the inverse solution X to equation (9) also will be straightforward. There are many well established methods for regularizing this ill-conditioned problem, e.g., Tikhonov regularization and singular value decomposition method. Here we simply employed the built-in function "lsqr" in Matlab (The MathWorks, Inc.) to solve the least square problem using Gausss-Newton algorithm:

$$\min_X(\|Y - AX\| + \rho\|LX\|) \quad (10)$$

Here ρ is regularization parameter, and L is regularization matrix.

2.2. Reconstruction of atrial endocardial surface

The atria from a normal crossbred sheep heart (45 Kg) were scanned using a 4.7T Varian Magnetic Resonance imaging (MRI) scanner operated by the Centre for Advanced Magnetic Resonance Imaging (CAMRI), University of Auckland. Atrial image stacks were obtained at 300 µm in-plane and 500 µm **z** resolution. Figure 2 displays the original MR image stack and reconstructed atrial surface structure.

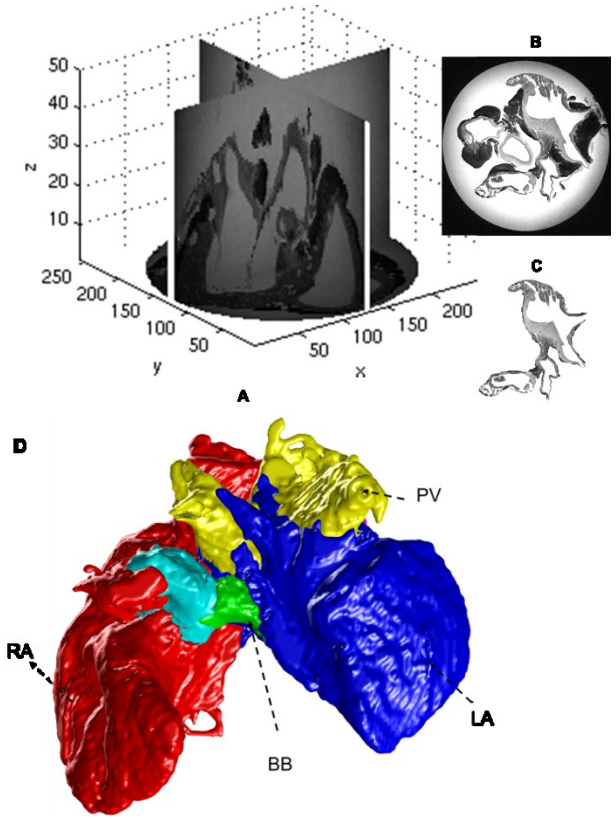

Figure 2: (A) Three orthogonal views of the MR image stack. The raw images (B) were segmented (C) and used to reconstruct 3D surface geometry of atria. (D) 3D reconstruction of antero-superior view of the atrial epicardial surface. Here, RA = right atrium; LA = left atrium; BB = Bachman's bundle; PV = pulmonary veins.

However, what we really need is the endocardial surface of one atrial chamber , e.g., LA, and the locations of 64 catheters to test the difference in potentials between them by employing forward and inverse problems. CTMRedit [12] was used for extracting the endocardial surface and creating the 64 locations of catheters. Figure 3A displays how we selected the boundary on each 2D MRI image using CTMRedit and Figure 3B illustrates the 64 electrodes of the MEA inside the LA endocardial surface.

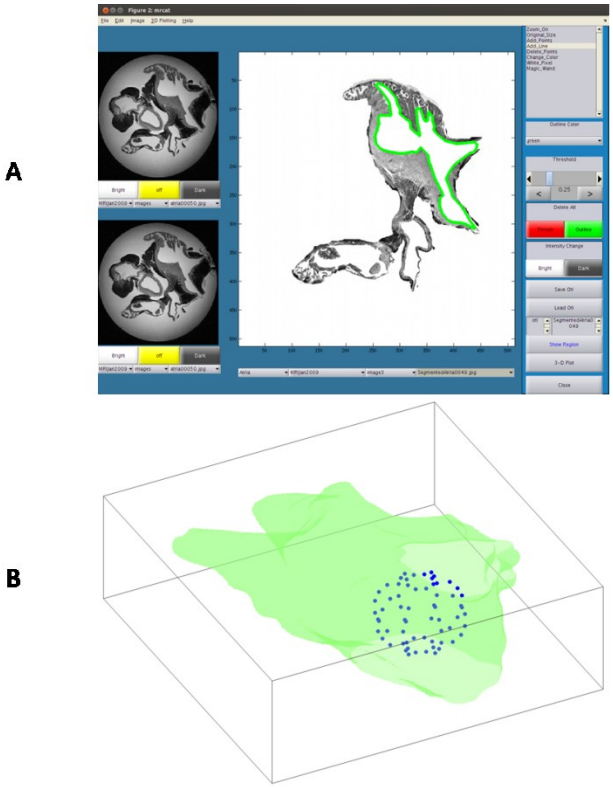

Figure 3: (A) Extracting endocardial surface of LA using CTMRedit. Here take a 2D atrial MRI image as an example, the closed green line displays LA contour. (B) Reconstructed LA endocardium, the 64 blue dots indicate locations of MEA. Here LAA = left atrial appendage; PV = pulmonary veins.

2.3. Forward solution using atrial structure

It may be slightly challenging to extend the FDM approach in Section 2.1 to 3D realistic problem. One possible obstacle is how to estimate normal directions at complex 3D object. In this study, a novel structure tensor approach [13] was used to obtain surface normal direction for the 3D object in order to discretize Neumann boundary equation (3). Figure 4 displays normal directions (red lines) obtained by structure tensor at a 2D ring (black dots) of 3D object.

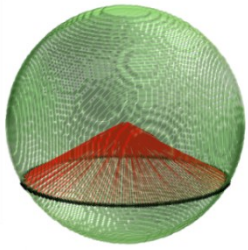

Figure 4: Normal directions (red lines) by structure tensor displayed at a 2D ring (black dots) of 3D object.

We set up an experiment using the endocardial surface of LA and MEA in which forward solution will be used.

3. Results

The forward and inverse problems for equation (1) have been solved. Figure 5I-A displays the initial inputs for the test forward problem (red line), and the forward solutions are displayed at the 5×5 grid points in Figure 1B. Figure 5I-A gives the output (in blue) of the inverse problem using the previous forward solution as inputs. Figure 5I-B demonstrates the error between the "true source" and predicted source, which is the order of spatial discretizing step h.

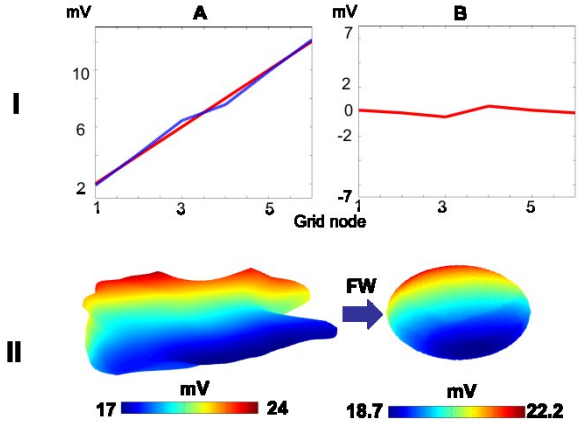

Figure 5: **I**) Forward and inverse solutions for the 2D test problem are displayed. (**A**) Initial inputs for the forward solution are in red and the output for inverse problem in blue. (**B**) Errors between the source and predicted sources. **II**) A forward problem was applied on the LA and MEAs.

Figure 5IIA-B displays the initial input and output for forward problem using realistic 3D atrial structure, respectively. We can see the results are quite consistent between the input and output.

4. Conclusions and future work

This work has studied the relationship between potentials recorded at MEAs and actual ones on atrial endocardial surface by exploring the forward and inverse problems in a nutshell. We confirm that forward and inverse solutions are a robust approach to project potentials between the different objects. In future, we will use well established forward/inverse package, e.g., Scirun. Furthermore, we will employ high resolution human CT data to reconstruct atrial structure.

Acknowledgements

This work is supported by China Scholarship Council and University of Auckland Joint Scholarships, Health Research Council of New Zealand (NZ), National Heart Foundation of NZ (No 1477), Performance-Based Research Fund, University of Auckland, NZ.

References

[1] Lloyd-Jones DM, Wang TJ, Leip EP, Larson MG, Levy D, Vasan RS, D'Agostino RB, Massaro JM, Beiser A, Wolf PA, Benjamin EJ. Lifetime risk for development of atrial fibrillation: the Framingham Heart Study. Circulation 2004; 110(9):1042-6.

[2] Bunch TJ et al.. Patients treated with catheter ablation for atrial fibrillation have long-term rates of death, stroke, and dementia similar to patients without atrial fibrillation. J Cardiovasc Electrophysiol 2011;22:839-45.

[3] Brooks AG, Stiles MK, Laborderie J, Lau DH, Kuklik P, Shipp NJ, Hsu L, P. Sanders P. Outcomes of long-standing persistent atrial fibrillation ablation: a systematic review. Heart Rhythm, 2010;7: 835-846.

[4] Chao TF, Tsao HM, Lin YJ, et al. Clinical outcome of catheter ablation in patients with nonparoxysmal atrial fibrillation: results of 3-year follow-up. Circ. A&E., 2012;5:514-20.

[5] Iwasaki Y-K, Nishida K, Kato T, Nattel S. Atrial fibrillation pathophysiology: Implications for management. Circulation. 2011;124:2264-2274.

[6] Skadsberg ND, He B, Laske, Laizzo PA. Cardiac mapping technology. Handbook of Cardiac Anatomy,Physiology, and Devices edited by P.A. Iaizzo, Springer, 2009.

[7] Multielectrode basket catheter. Australia and New Zealand Horizon Scanning Network, 2010.

[8] Narayan SM, Krummen DE, & Rappel WJ. Clinical mapping approach to diagnose electrical rotors and focal impulse sources for human atrial fibrillation. J Cardiovasc Electrophysiol, 2012; 23:447-54.

[9] Ector J, De Buck S, Huybrechts W, et al. Biplane three-dimensional augmented fluoroscopy as single navigation tool for ablation of atrial fibrillation: accuracy and clinical value. Heart Rhythm. 2008 ;5(7):957-64.

[10] Burton BM, Tate JD, Erem B, Swenson DJ, Wang DF, Steffen M, Brooks DH, Dam PM, Macleod RS. A Toolkit for Forward/Inverse Problems in Electrocardiography within the SCIRun Problem Solving Environment. 33rd Annual International Conference of the IEEE EMBS Boston, USA, 2011.

[11] Zhao J, Davison M, Corless RM. Compact finite difference method for American option pricing. Journal of Computational and Applied Mathematics, Vol. 206(1), 2007, 306-321.

[12] CTMRedit. www.ee.ucla.edu/~spapl/CTMRedit.

[13] Zhao J, Butters TD, Zhang H, Pullan, AJ, LeGrice IJ, Sands GB, Smaill BH. An image-based model of atrial muscular architecture: Effects of structural anisotropy on electrical activation. Circulation: A.&E., 2012;5:361-370.

Address for correspondence

Dr. Jichao Zhao, Auckland Bioengineering Institute, University of Auckland,Auckland, 1142, New Zealand.
E-mail: j.zhao@auckland.ac.nz